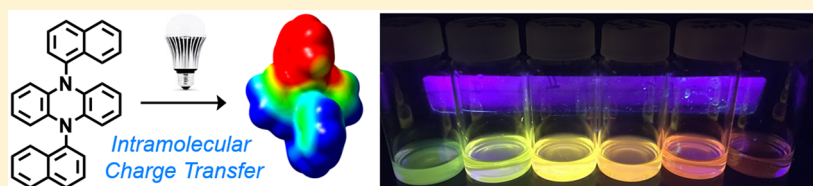# Intramolecular Charge Transfer and Ion Pairing in *N,N*-Diaryl Dihydrophenazine Photoredox Catalysts for Efficient Organocatalyzed Atom Transfer Radical Polymerization

Chern-Hooi Lim,[†,∥] Matthew D. Ryan,[†,∥] Blaine G. McCarthy,[†] Jordan C. Theriot,[†] Steven M. Sartor,[†] Niels H. Damrauer,[†,§] Charles B. Musgrave,[†,‡,§] and Garret M. Miyake*[,†,§]

[†]Department of Chemistry and Biochemistry, [‡]Department of Chemical and Biological Engineering, and [§]Materials Science and Engineering Program, University of Colorado Boulder, Boulder, Colorado 80309, United States

S *Supporting Information*

ABSTRACT: Photoexcited intramolecular charge transfer (CT) states in *N,N*-diaryl dihydrophenazine photoredox catalysts are accessed through catalyst design and investigated through combined experimental studies and density functional theory (DFT) calculations. These CT states are reminiscent of the metal to ligand charge transfer (MLCT) states of ruthenium and iridium polypyridyl complexes. For cases where the polar CT state is the lowest energy excited state, we observe its population through significant solvatochromic shifts in emission wavelength across the visible spectrum by varying solvent polarity. We propose the importance of accessing CT states for photoredox catalysis of atom transfer radical polymerization lies in their ability to minimize fluorescence while enhancing electron transfer rates between the photoexcited photoredox catalyst and the substrate. Additionally, solvent polarity influences the deactivation pathway, greatly affecting the strength of ion pairing between the oxidized photocatalyst and the bromide anion and thus the ability to realize a controlled radical polymerization. Greater understanding of these photoredox catalysts with respect to CT and ion pairing enables their application toward the polymerization of methyl methacrylate for the synthesis of polymers with precisely tunable molecular weights and dispersities typically lower than 1.10.

■ INTRODUCTION

Visible light photoredox catalysis presents a platform for greener chemistries through the use of solar energy to drive chemical transformations under mild conditions.[1] Photoredox catalysis has been successfully applied in polymer synthesis for the production of well-defined polymers through controlled radical polymerization (CRP) mechanisms, including reversible addition–fragmentation transfer (RAFT),[2] reversible complexation mediated living radical polymerization (RCMP),[3] and atom transfer radical polymerization (ATRP).[4] CRPs have greatly impacted polymer synthesis, providing methodologies to produce well-defined polymers under experimentally accessible and versatile reaction conditions.[5] Among all CRPs, ATRP has become the most studied method.[6] In ATRP, the catalyst's control over the equilibrium between a dormant alkyl halide and the active propagating radical maintains a low concentration of radicals in solution to minimize bimolecular termination pathways and enable the synthesis of well-defined polymers with low dispersity (Đ).

Ruthenium,[7] copper,[8] iron,[9] and iridium[10] complexes have been used as photoredox catalysts (PCs) in ATRP; however, most PCs do not possess a sufficiently negative reducing potential to directly reduce an alkyl bromide (e.g., ∼ −0.8 V vs SCE for ethyl *α*-bromophenylacetate)[11] ATRP initiator through an outer sphere electron transfer mechanism, necessitating the addition of a sacrificial electron donor for the polymerization to proceed through a reductive quenching pathway; such sacrificial electron donors introduce undesirable reaction pathways[12] that make the synthesis of polymers with low Đ challenging.[13] Photoexcited states of certain strongly reducing iridium[10] and copper[8] PCs can directly reduce an alkyl bromide via the oxidative quenching pathway, eliminating the need for sacrificial electron donors and enabling the synthesis of well-defined polymers. However, concerns are raised regarding sustainability of precious metals[14] and trace metal contamination that can impede use of the resulting materials, for example in electronic applications. Although extensive efforts to develop purification techniques and catalyst strategies have succeeded in reducing transition metal contamination,[15] a more direct route to eliminate this issue is the development of organocatalyzed-ATRP (O-ATRP) (Figure 1).
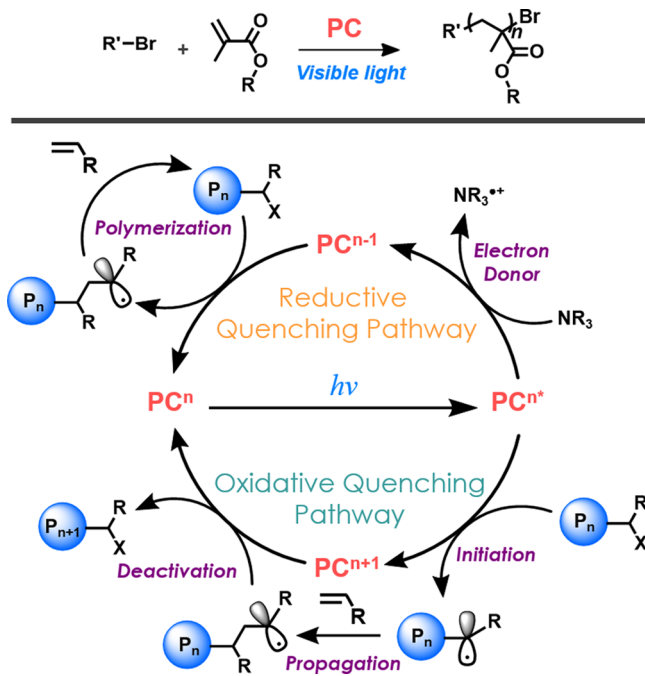
Figure 1. Photoredox mediated O-ATRP of polar vinyl monomers with an alkyl bromide initiator can proceed through either a reductive (top) or oxidative quenching pathway (bottom).

Similar to metal complexes, organic PCs[16] that directly reduce alkyl bromide bonds are less common. However, perylene,[17] N-arylphenothiazines,[18] N,N-diaryl dihydrophenazines,[19] and N-arylphenoxazines[20] (Figure 2) have all been

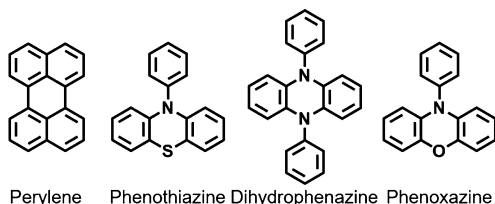Perylene   Phenothiazine   Dihydrophenazine   Phenoxazine

Figure 2. Structures of strongly reducing organic photoredox catalysts used in O-ATRP.

reported as organic PCs for ATRP, proceeding through an oxidative quenching pathway. Our recent work in this field has involved using computational quantum chemical catalyst design and analysis to understand the intricacies of the polymerization mechanism to enable further advancements toward the realization of more efficient organic PCs. Furthermore, we have striven to design PCs that operate in the visible spectrum in order to minimize UV light-induced side reactions and develop energy efficient polymerization methodologies. For example, theoretical insight led to the discovery of a core substituted N-aryl phenoxazine as an efficient visible light organic PC for the O-ATRP for the synthesis of poly(methyl methacrylate) (PMMA) with tailored molecular weights (MWs) and low Đ while achieving high initiator efficiencies (I*s).[20]

Our previous studies using N,N-diaryl dihydrophenazines and N-aryl phenoxazines revealed that PCs with lowest energy excited states possessing quantum chemically predicted charge separated singly occupied molecular orbitals (SOMOs) exhibited superior performance in O-ATRP compared to

those possessing SOMOs that are both localized on either the dihydrophenazine or phenoxazine core. The predicted charge separated SOMOs suggest the occurrence of intramolecular CT in their lowest triplet excited state. The CT nature of dihydrophenazines and phenoxazines has also been recognized as an important feature in the design of organic light emitting diodes.[21] Here, we substantiate the CT nature of diaryl dihydrophenazines with experimental and computational data and hypothesize on the necessity of the CT state for efficient O-ATRP.
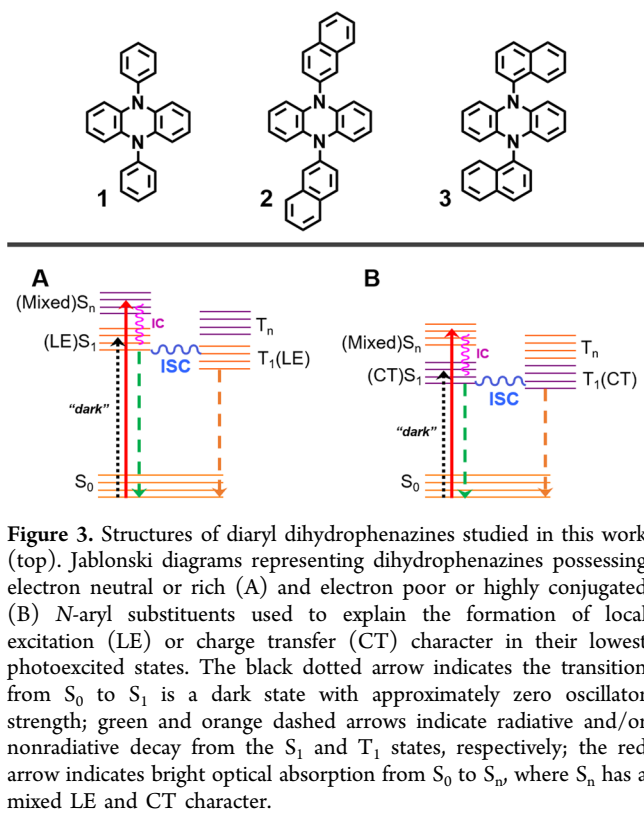
DFT calculations predict that for dihydrophenazines with N-aryl substituents possessing extended conjugation (e.g., naphthalene) or phenyl substituents functionalized with electron withdrawing groups, the N-aryl substituents' lowest energy π* orbital becomes the lowest unoccupied molecular orbital (LUMO) of the dihydrophenazine molecule, suggesting that the lowest energy excited state possesses CT character. These predictions are supported by the experimental observation that these types of molecules exhibit significant solvatochromic shifts in emission (vide infra), spanning wavelengths from blue (in nonpolar 1-hexene) to red (in polar dimethylformamide, DMF). In contrast, the dihydrophenazine possessing the less conjugated and unfunctionalized phenyl N-aryl substituent possesses a LUMO that is localized on the dihydrophenazine core. Dihydrophenazines of this nature possess nonpolar lowest energy excited states that are localized excitations and do not display solvatochromism, emitting blue light regardless of solvent polarity.

These results corroborate DFT predictions that charge separated SOMOs correspond to intramolecular CT in the lowest excited state and that the observed increasing solvatochromic red-shift in emission with increasing solvent polarity is due to stabilization of the polar CT state. The direction of the intramolecular CT is from the electron rich dihydrophenazine core to the lowest lying π* orbital of the N-aryl substituent, which is reminiscent of the metal to ligand charge transfer (MLCT) states of polypyridyl ruthenium and iridium PCs[22] and the proposed CT state of 9-mesityl-10-methylacridinium.[23]

We posit that intramolecular CT in the lowest lying excited state of N,N-diaryl dihydrophenazine PCs minimizes fluorescence and enables fast electron transfer. Herein, we further investigate the formation of dihydrophenazine CT states in solvents of varying polarity and elucidate their importance for O-ATRP performance using a combined computational and experimental approach. Holistic consideration of the O-ATRP mechanism and the influences imparted by solvent polarity are shown to affect the interplay between the nature of the PC's CT character as well as the free energy of ion pair binding between the PC radical cation and bromide anion, which is crucial in the deactivation step and thus obtaining desirable O-ATRP results. This insight into the effects of solvent polarity and subsequent optimization of reaction conditions to encourage efficient activation and deactivation allows for the synthesis of PMMA with Đ typically below 1.10 and quantitative initiator efficiencies (I*s).

■ RESULTS AND DISCUSSION

Three representative diaryl dihydrophenazine based PCs possessing phenyl (**1**), 2-naphthalene (**2**), and 1-naphthalene (**3**) N-aryl substituents were investigated for their ability to form CT states and their associated potential influences on their O-ATRP performance (Figure 3). Our proposed

Figure 3. Structures of diaryl dihydrophenazines studied in this work (top). Jablonski diagrams representing dihydrophenazines possessing electron neutral or rich (A) and electron poor or highly conjugated (B) N-aryl substituents used to explain the formation of local excitation (LE) or charge transfer (CT) character in their lowest photoexcited states. The black dotted arrow indicates the transition from S_0 to S_1 is a dark state with approximately zero oscillator strength; green and orange dashed arrows indicate radiative and/or nonradiative decay from the S_1 and T_1 states, respectively; the red arrow indicates bright optical absorption from S_0 to S_n, where S_n has a mixed LE and CT character.

mechanism of O-ATRP hinges on the ability of the photo-excited PC to access the triplet excited state (^{3}PC*) via intersystem crossing (ISC), which may be of local excitation (LE) or of CT character, depending on the relative energies of the π^* orbitals of the dihydrophenazine core and the N-aryl substituents. Thereafter, ^{3}PC* can reduce an alkyl halide to generate the active propagating radical and the ion pair between the oxidized PC (^{2}PC$^{\bullet+}$) and bromide (Br$^-$). Finally, the

propagating radical must be efficiently deactivated by the ^{2}PC$^{\bullet+}$Br$^-$ ion pair to complete the catalytic cycle. A Jablonski diagram for PCs that possess lowest energy excited states with LE or CT character is schematically represented in Figures 3A and 3B. Time-dependent DFT (TD-DFT) calculations and ultraviolet–visible (UV–vis) spectroscopy were used to evaluate the nature of the initial photoexcitation event (Figure 4).[24] Interestingly, TD-DFT calculations reveal that the initial photoexcitation of PC **1** involves mixed CT and LE characters, although the dark, fully relaxed, lowest singlet and triplet excited states are exclusively of LE character (Figure 5).

TD-DFT calculations of PC **1** predict that the lower energy $S_0 \rightarrow S_1$ excitation dominantly possesses $\pi_{HOMO}-\pi_{LUMO}$ character and is dark with zero oscillator strength (f). However, the $S_0 \rightarrow S_2$ excitation is predicted to be bright with a maximum wavelength ($\lambda_{max,abs}$) of 369 nm, $f = 0.229$, and contributions of 82% from the $\pi_{HOMO}-\pi_{LUMO+1}$ and 12% from the $\pi_{HOMO}-\pi_{LUMO+7}$ transitions (Figure 4A). The $\pi_{HOMO}-\pi_{LUMO+1}$ transition is of CT character, where an electron occupying PC **1**'s HOMO, which is a π orbital localized on the phenazine core ($\pi_{core} = \pi_{HOMO}$), is promoted into the spatially separated N-substituent's π^*_{phenyl} LUMO + 1 orbital (π_{LUMO+1}). On the other hand, the $\pi_{HOMO}-\pi_{LUMO+7}$ transition is of LE character, involving only π_{core} (π_{HOMO}) and π^*_{core} (π_{LUMO+7}). In the absence of π^*_{phenyl}, such as in the case of 5,10-dimethyl-5,10-dihydrophenazine, only one peak of exclusively LE character is observed at a blue-shifted $\lambda_{max,abs}$ of 337 nm.[25]

After initial photon absorption, fast relaxation via internal conversion (IC) results in thermalization of the excited electron from S_2 (π_{LUMO+1} and π_{LUMO+7}) to the lowest singlet excited state S_1 (π_{LUMO}), followed by ISC to the lowest triplet excited state (T_1) comprised of exclusively LE character (Figure 5A). The triplet quantum yield of PC **1** has been reported to be 0.26 at 77 K in 3-methylpentane.[25] Further, the electrostatic potential (ESP)-mapped electron density reveals minimal dipole moment (μ) change for PC **1** as it transitions from the ground state (^{1}PC) to ^{3}PC*, despite the slight increase in
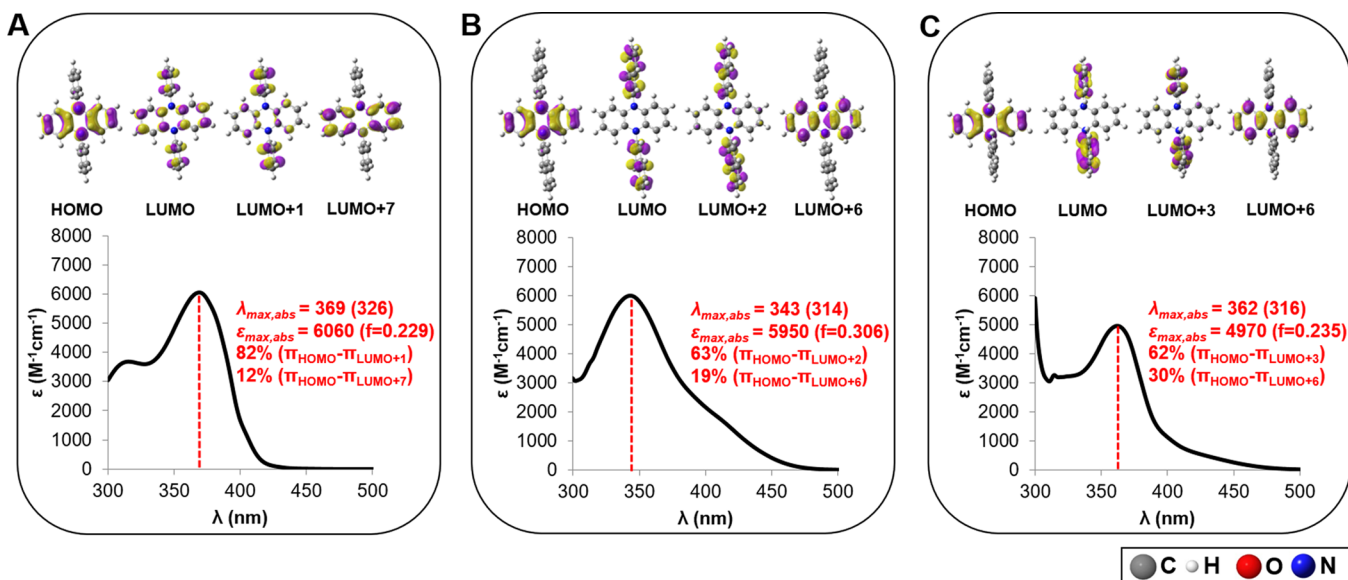

Figure 4. Ultraviolet–visible (UV–vis) spectrum of N,N-diaryl dihydrophenazines **1** (A), **2** (B), and **3** (C) along with theoretically assigned percentage contributions (>10%) of various orbitals to the observed absorption peaks. $\lambda_{max,abs}$ is the absorption maximum wavelength in units of nm, and $\varepsilon_{max,abs}$ is the molar absorptivity at $\lambda_{max,abs}$ in units of M^{-1} cm^{-1}; both are measured in dimethylacetamide (DMA) solvent. $\lambda_{max,abs}$ and oscillator strength (f) values predicted at the TD-DFT CAM-B3LYP/6-31+G(d,p)/CPCM-DMA level of theory are enclosed in parentheses for comparison.
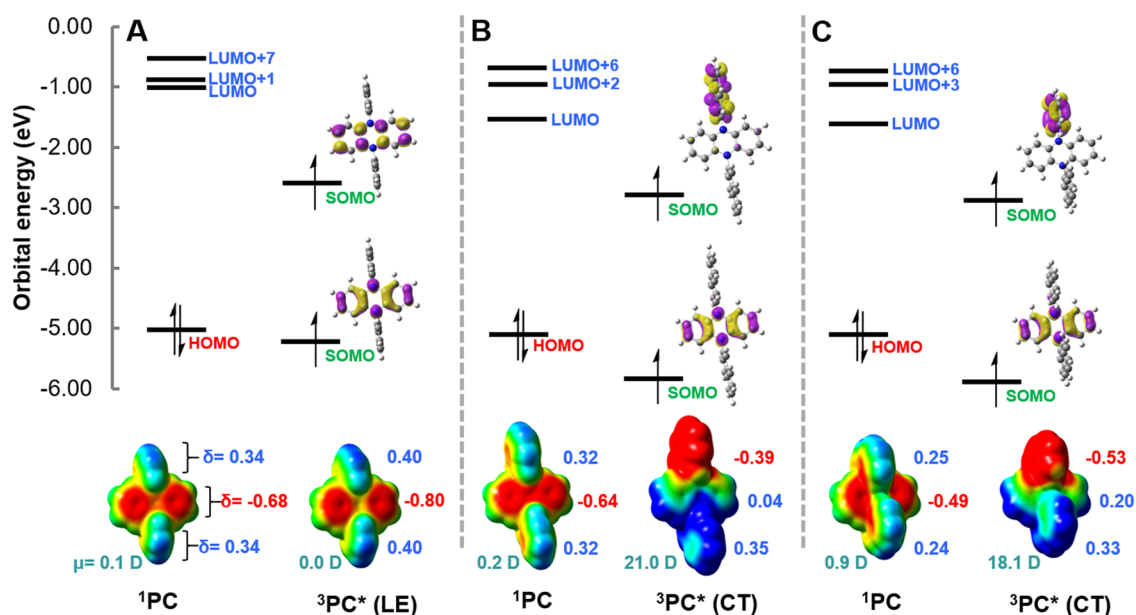
Figure 5. Orbital energy (in eV) of ^{1}PC (HOMO and LUMOs) and ^{3}PC* (SOMOs) of *N,N*-diaryl dihydrophenazines **1** (A), **2** (B), and **3** (C); HOMO = highest occupied molecular orbital, LUMO = lowest unoccupied molecular orbital, SOMO = singly occupied molecular orbital, ^{1}PC = photocatalyst's ground state, ^{3}PC* = photocatalyst's lowest triplet state. Computed partial charge (δ, in units of e) using the electrostatic potential (ESP) CHELPG formalism. ESP-mapped electron density (displayed at the bottom): "red" indicates electron rich regions, while "blue" indicates electron poor regions. Computed dipole moment (μ) in units of Debye (D).
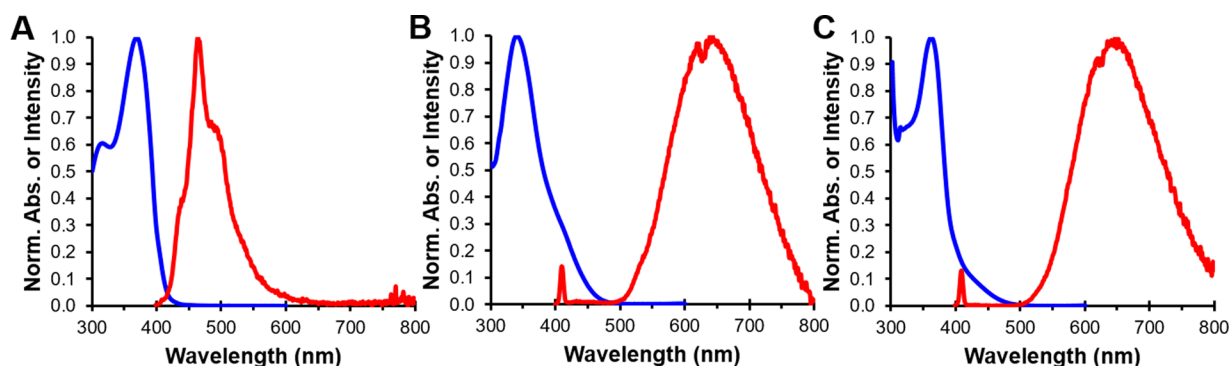

Figure 6. Overlaid absorption (blue) and emission (red) spectra of PCs **1** (A), **2** (B), and **3** (C) in DMA.

electron density on the core from $\delta = -0.68$e to -0.80e (Figure 5A).

Similar to PC **1**, the initial photon absorption by PCs **2** and **3** consists of a combination of CT and LE character (Figures 4B and C). For PC **2**, the $\lambda_{max,abs}$ at 343 nm is assigned to be the $S_0 \rightarrow S_4$ excitation with $f = 0.306$ and consists of 63% of the $\pi_{HOMO}-\pi_{LUMO+2}$ (CT character) and 19% of the $\pi_{HOMO}-\pi_{LUMO+6}$ (LE character) transitions (Figure 4B). While for PC **3**, the $\lambda_{max,abs}$ at 362 nm is similarly assigned to be the $S_0 \rightarrow S_4$ excitation with $f = 0.235$ and composed of 62% of the $\pi_{HOMO}-\pi_{LUMO+3}$ (CT character) and 30% of the $\pi_{HOMO}-\pi_{LUMO+6}$ (LE character) transitions (Figure 4C). Following photon absorption, fast IC from S_4 (high-lying π^*) to S_1 (π_{LUMO}) occurs for both PC **2** and **3**.

In contrast to PC **1**, the LUMOs of PCs **2** and **3** are exclusively π^* orbitals of the *N*-naphthalene substituent (Figure 4) and are lower in energy relative to the LUMO of PC **1** by 0.57 and 0.66 eV, respectively (Figure 5). As such, during IC to the S_1 state, PCs **2** and **3**'s $\pi^*_{naphthyl}$ LUMO will be populated to first form the CT S_1 state, which upon ISC results in the CT T_1 state composed of the charge separated SOMOs (Figures 5B

and 5C). The electrostatic potential (ESP)-mapped electron density highlights the CT character and large dipole moments of 21.0 and 18.1 D for PCs **2** and **3**'s ^{3}PC* state, respectively (Figures 5B and C). For extended details of Figure 4, see Figure S1.

The LE nature of PC **1**'s and the CT nature of PC **2** and **3**'s lowest excited states are further supported through examination of their absorption and emission spectra (Figure 6). In PC **1**, the thermal relaxation of the excited electron from S_2 to S_1 results in a Stokes shift of 98 nm with emission spectra possessing rather sharp features. In contrast, for PCs **2** and **3**, much broader and featureless peaks and larger Stokes shifts of 311 and 301 nm, respectively, are observed due to the relaxation of the excited electron from S_4 into the much lower energy LUMO (relative to PC **1**'s LUMO) of S_1 stabilized by electron delocalization of the extended $\pi^*_{naphthalene}$ orbital. We suggest that the observed emission spectra in Figure 6 are predominantly due to direct fluorescence from the lowest singlet excited state. This assignment is made because introduction of oxygen to such samples results in a minimal quenching of the emission (Figure S9). It is worth noting that
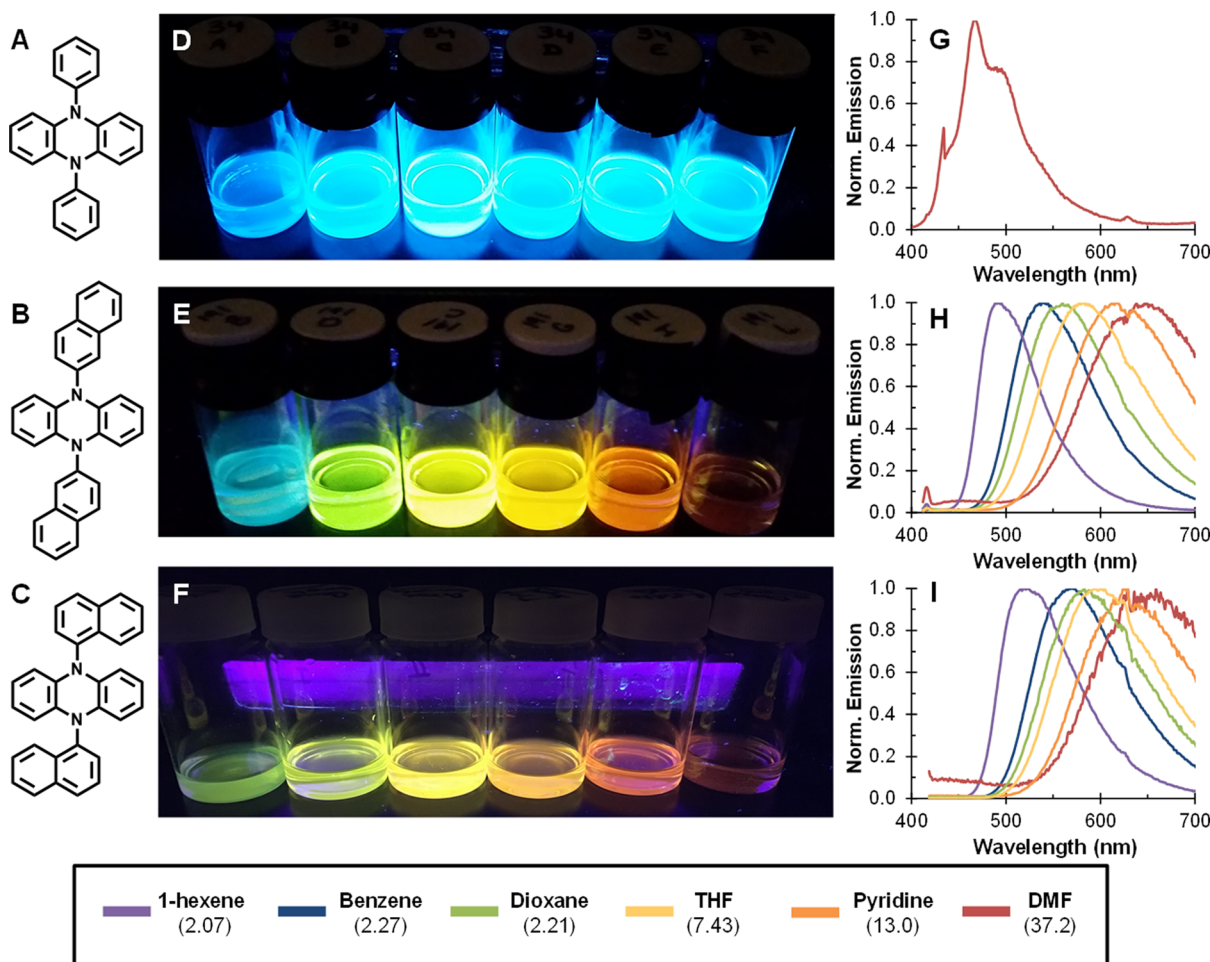
Figure 7. Structures of diaryl dihydrophenazines with LE (A) or CT (B and C) natures. Photographs of solutions of the diaryl dihydrophenazines upon excitation with 365 nm light (D, E, and F) and their emission spectra (G, H, and I) in solvents with varying polarity. For D−F, the order of solvents from left to right (dielectric constant, ε) is as follows: 1-hexene (ε = 2.07), benzene (ε = 2.27), dioxane (ε = 2.21), THF (ε = 7.43), pyridine (ε = 13.0), and DMF (ε = 37.2).

the fluorescence wavelength from the CT singlet state can be used to estimate the energy of the CT lowest triplet state, as the energies of the CT lowest singlet and triplet states are expected to be nearly degenerate.[21,26]

Due to the large differences in computed LE or CT characters, dipole moments, and observed emission spectra for PCs **1** versus **2** or **3**, we reasoned that increased solvent polarity would significantly stabilize the polar S_1(CT) state of **2** and **3** (and thus red-shift the emission wavelength) and minimally stabilize the nonpolar S_1(LE) state of **1**. To test this hypothesis, the emission profiles of these dihydrophenazines were investigated in solvents possessing a range of polarities. These experiments validate the predicted striking contrast in the dihydrophenazine derivatives. Emission remains essentially unchanged for PC **1**, whereas, for PCs **2** and **3**, a large solvatochromic effect in emission is observed, with the maximum wavelength ($\lambda_{max,em}$) spanning nearly the entire visible spectrum (Figure 7). This solvatochromic response is attributed to emission from polar S_1(CT) states of PCs **2** and **3**, which are stabilized in more polar solvents, resulting in increasingly larger Stokes shifts and therefore red-shifted emission (see Figure S7 for further details).

Using the observed Stokes shifts in various solvents and the Lippert equation,[27] the change in dipole moment ($\Delta\mu$) from S_1(CT) to S_0 of PCs **2** and **3** was estimated to be 22.1 and 16.0

D, respectively (Figures S3 and S4). These experimentally derived $\Delta\mu$ values corroborate the DFT-predicted $\Delta\mu$ values (estimated from the T_1 state possessing similar CT character). For PCs **2** and **3**, the predicted $\Delta\mu$ values are 20.8 D [e.g., 20.8 D = 21.0 D (^{3}PC*) − 0.2 D (^{1}PC)] and 17.2 D, respectively (Figures 5B and C). The large $\Delta\mu$ values for PCs **2** and **3** between the ground state and the lowest excited state, along with their broad and featureless emission profiles, strongly suggest that PC **2** and **3**'s lowest excited states are CT in character.[28] Combined, these data indicate that PC **1**'s lowest excited state is of LE character while for PCs **2** and **3**, which possess low-lying $\pi^*_{naphthalene}$ LUMOs, the lowest excited state has CT character with extraordinary sensitivity to solvent polarity.

In light of the strong influence of solvent polarity on the emission profiles of PCs **2** and **3**, we reasoned that solvent polarity would greatly influence catalyst performance in polymerization reactions from multiple perspectives. Performing polymerizations in polar solvents effectively stabilizes the ^{3}PC* of CT complexes, which decreases the reducing power of the PC. Even more influential when considering the entire O-ATRP mechanism, the polarity of the solvent would be expected to significantly influence the ion pairing of ^{2}PC$^{\bullet+}$Br$^-$ and, thus, affect its formation, binding energy, lifetime, and, thus, ability to deactivate the propagating radical efficiently

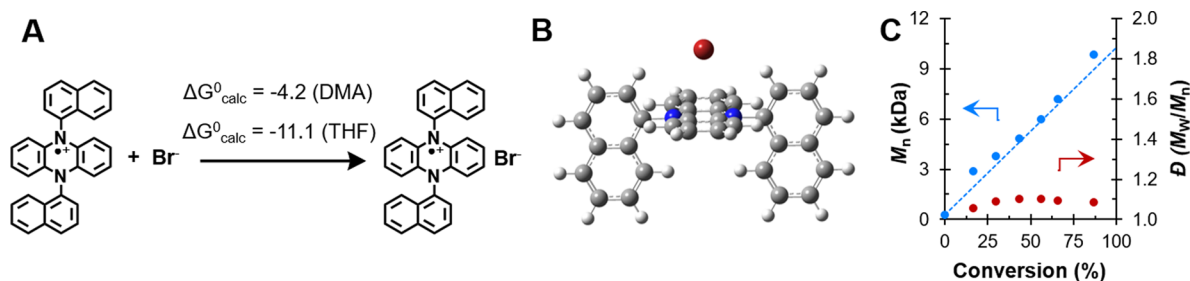**Figure 8.** Solvent effects on the ion pairing of ^{2}PC$^{\bullet+}$ and Br$^-$ (A). Optimized geometry of the ^{2}PC$^{\bullet+}$Br$^-$ pair (B). (C) Plot of M_n and Đ as a function of monomer conversion for the polymerization of MMA in 3:1 DMA:THF. The dashed line represents the theoretical M_n growth.

(*vide infra*).[29] In short, the appropriate polarity of the reaction medium is required to balance all of these properties to achieve an optimal polymerization synthesis through O-ATRP.

Efficient deactivation minimizes bimolecular termination of active propagating radicals ($P_n^{\bullet}$) and is critical for controlled O-ATRP. Deactivation of O-ATRP requires oxidation of $P_n^{\bullet}$ by ^{2}PC$^{\bullet+}$Br$^-$ to reinstall the bromine chain-end group to regenerate ^{1}PC and P_n-Br (Figure S8). This deactivation step is formally a three-body event requiring $P_n^{\bullet}$, ^{2}PC$^{\bullet+}$, and Br$^-$ to come together via random diffusion to produce a productive collision; however, such three-body events are entropically improbable, especially considering the low concentrations of these species. Therefore, we hypothesize that ion pairing of ^{2}PC$^{\bullet+}$ and Br$^-$ to form ^{2}PC$^{\bullet+}$Br$^-$ is essential for effective deactivation because it reduces a three-body collision to a more likely pseudo-two-body collision event involving only ^{2}PC$^{\bullet+}$Br$^-$ and $P_n^{\bullet}$.

We studied this ion pair using DFT (Figure S2) to calculate the standard complexation Gibbs free energy ($\Delta G^0_{complex}$) for ^{2}PC$^{\bullet+}$Br$^-$ formation in DMA and the less polar THF, shown in Figure 8A. For PC **3**, the formation of ^{2}PC$^{\bullet+}$Br$^-$ in DMA is predicted to be exergonic ($\Delta G^0_{complex}$ = −4.2 kcal/mol). However, its formation is even more favorable in the less polar THF solvent ($\Delta G^0_{complex}$ = −11.1 kcal/mol).[24] The optimized geometry of the ^{2}PC$^{\bullet+}$Br$^-$ complex consists of the bromide anion residing on the center of the dihydrophenazine core (the positive charge of ^{2}PC$^{\bullet+}$ localizes the anion) ∼ 3.5 Å from each nitrogen (Figure 8B). In short, modulation of the strength of ion pairing between ^{2}PC$^{\bullet+}$ and Br$^-$ by conducting the polymerization in a medium with optimal polarities enhances the capability of these PCs to produce polymers with controlled MWs and low Đ.

To test the combined effects of solvent polarity on overall catalyst performance in polymerization, PC **3** was used to polymerize MMA in mixed solvent systems comprised of various percentages of DMA (ε = 37.8) and THF (ε = 7.58) to systematically alter the overall dielectric constant (ε) of the overall reaction medium (Table S1, Figures S5 and S6). These experiments reveal that the best overall MMA polymerization performance is obtained using a 3:1 volume:volume ratio of DMA to THF, to produce polymers with the combination of lowest Đ and highest I^*. Using diethyl 2-bromo-2-methylmalonate (DBMM) as the initiator results in the production of PMMA with Đ = 1.08 and a nearly quantitative I^* of 91.2%, while exhibiting a highly linear increase in polymer MW as a function of monomer conversion (Figure 8C).

Using this mixed solvent system allows for the synthesis of polymers with target MWs and low Đ through modulation of either the initiator or monomer in the overall stoichiometry of the reaction (Table 1). In comparison, using only DMA as the

solvent results in the production of PMMA with higher dispersity (Đ = 1.16) and decreased control over MW (I^* = 79.7%). The enhanced control over the polymerization through manipulation of the solvent polarity further validates the proposed O-ATRP mechanism, although the improvements in polymerization performance could be attributed to influences in both the activation (i.e., nature of the CT states) and deactivation steps. Combined, these effects are macroscopically observed in that the rate of polymerization decreases with decreasing polarity of the reaction medium.

Table 1. Solvent Effects on the Ion Pairing of ^{2}PC$^{\bullet+}$Br$^-$ and Results for the Polymerization of MMA in DMA:THF[a]

Run No.	[MMA]: [DBMM]:[3]	Conversion (%)[b]	M_w (kDa)[c]	M_n (kDa)[c]	Đ (M_w/ M_n)[c]	I^* (%)[d]
1	1000:5:1	81.7	18.9	16.2	1.16	102
2	1000:10:1	86.8	10.6	9.8	1.08	91.2
3	1000:15:1	83.2	5.55	5.15	1.08	113
4	1000:20:1	76.4	4.67	4.29	1.09	95.1
5	500:10:1	94.8	5.20	4.77	1.09	105
6	750:10:1	93.1	6.67	6.07	1.10	119

[a]See Supporting Information for details. [b]Measured by ^{1}H NMR. [c]Measured by GPC coupled with light scattering. [d]I^* = theoretical number-average MW/experimentally measured number-average MW × 100. DMA:THF = 3:1 (v:v).

■ CONCLUSIONS

Factors affecting how *N,N*-diaryl dihydrophenazine photoredox catalysts access photoexcited intramolecular charge transfer states have been studied through a combined experimental and computational approach, and the importance of this state in the proposed polymerization mechanism has been hypothesized. Solvent polarity has proven to be an influential parameter for polymerization, affecting both the degree of charge transfer in the excited states of the photoredox catalyst as well as the ion pairing between the catalyst radical cation and the bromide anion. These combined factors hone our understanding of the polymerization mechanism, and this has enabled the synthesis of well-defined poly(methyl methacrylate) with dispersities typically less than 1.10 through organocatalyzed atom transfer radical polymerization. Increasing understanding of these organic photoredox catalysts has enabled the application of design principles to accelerate the development of these catalysts with superior properties, which we envision will have the potential to broadly replace unsustainable precious metal photoredox catalysts.

ASSOCIATED CONTENT

⑤ Supporting Information

The Supporting Information is available free of charge on the ACS Publications website at DOI: 10.1021/jacs.6b11022.

> Materials and methods; procedures; computational details; solvatochromic determination of dipole moment; supplementary catalyst characterization and polymerization data; coordinates of molecular structures (PDF)

AUTHOR INFORMATION

Corresponding Author

*garret.miyake@colorado.edu

ORCID ⓘ

Garret M. Miyake: 0000-0003-2451-7090

Author Contributions

‖C.-H.L. and M.D.R.contributed equally.

Notes

The authors declare no competing financial interest.

REFERENCES

(1) (a) Shaw, M. H.; Twilton, J.; MacMillan, D. W. C. *J. Org. Chem.* **2016**, *81*, 6898−6926. (b) Corrigan, N.; Shanmugam, S.; Xu, J.; Boyer, C. *Chem. Soc. Rev.* **2016**, *45*, 6165−6212. (c) Prier, C. K.; Rankic, D. A.; MacMillan, D. W. C. *Chem. Rev.* **2013**, *113*, 5322−5363. (d) Arias-Rotondo, D. M.; MuCusker, J. K. *Chem. Soc. Rev.* **2016**, *45*, 5803−5820. (e) Narayanam, J. M. R.; Stephenson, C. R. J. *Chem. Soc. Rev.* **2011**, *40*, 102−113. (f) Schultz, D. M.; Yoon, T. P. *Science* **2014**, *343*, 1239176-1−1239176-8.

(2) (a) McKenzie, T. G.; Fu, Q.; Uchiyama, M.; Satoh, K.; Xu, J.; Boyer, C.; Kamigaito, M.; Qiao, G. G. *Adv. Sci.* **2016**, *3*, 1500394. (b) Shanmugam, S.; Xu, J.; Boyer, C. *Angew. Chem., Int. Ed.* **2016**, *55*, 1036−1040. (c) Shanmugam, S.; Xu, J.; Boyer, C. *J. Am. Chem. Soc.* **2015**, *137*, 9174−9185. (d) Chen, M.; MacLeod, M. J.; Johnson, J. J. *ACS Macro Lett.* **2015**, *4*, 566−569. (e) Xu, J.; Shanmugam, S.; Duong, H. T.; Boyer, C. *Polym. Chem.* **2015**, *6*, 5615−5624. (f) Xu, J.; Jung, K.; Atme, A.; Shanmugam, S.; Boyer, C. *J. Am. Chem. Soc.* **2014**, *136*, 5508−5519.

(3) (a) Ohtsuki, A.; Lei, L.; Tanishima, M.; Goto, A.; Kaji, H. *J. Am. Chem. Soc.* **2015**, *137*, 5610−5617. (b) Ohtsuki, A.; Goto, A.; Kaji, H. *Macromolecules* **2013**, *46*, 96−102.

(4) Zivic, N.; Bouzrati-Zerelli, M.; Kermagoret, A.; Dumur, F.; Fouassier, J.-P.; Gigmes, D.; Lalevée, J. *ChemCatChem* **2016**, *8*, 1617−1631.

(5) (a) Matyjaszewski, K. *ACS Symp. Ser.* **2015**, *1187*, 1−17. (b) di Lena, F.; Matyjaszewski, K. *Prog. Polym. Sci.* **2010**, *35*, 959−1021. (c) Rosen, B. M.; Percec, V. *Chem. Rev.* **2009**, *109*, 5069−5119. (d) Moad, G.; Rizzardo, E.; Thang, S. H. *Acc. Chem. Res.* **2008**, *41*, 1133−1142. (e) Braunecker, W. A.; Matyjaszewski, K. *Prog. Polym. Sci.* **2007**, *32*, 93−146. (f) Kamigaito, M.; Ando, T.; Sawamoto, M. *Chem. Rev.* **2001**, *101*, 3689−3746. (g) Matyjaszewski, K. *ACS Symp. Ser.* **2000**, *768*, 2−26.

(6) (a) Boyer, C.; Corrigan, N. A.; Jung, K.; Nguyen, D.; Nguyen, T.-K.; Adnan, N. N. M.; oliver, S.; Shanmugam, S.; Yeow, J. *Chem. Rev.* **2016**, *116*, 1803−1949. (b) Matyjaszewski, K.; Tsarevsky, N. V. *J. Am. Chem. Soc.* **2014**, *136*, 6513−6533. (c) Matyjaszewski, K. *Macromolecules* **2012**, *45*, 4015−4039. (d) Ouchi, M.; Terashima, T.; Sawamoto, M. *Chem. Rev.* **2009**, *109*, 4963−5050. (e) Matyjaszewski, K.; Tsarevsky, N. V. *Nat. Chem.* **2009**, *1*, 276−288. (f) Ouchi, M.; Terashima, T.; Sawamoto, M. *Acc. Chem. Res.* **2008**, *41*, 1120−1132. (g) Matyjaszewski, K.; Xia, J. *Chem. Rev.* **2001**, *101*, 2921−2990.

(7) Zhang, G.; Song, I. Y.; Ahn, K. H.; Park, T.; Choi, W. *Macromolecules* **2011**, *44*, 7594−7599.

(8) (a) Ma, W.; Chen, D.; Ma, Y.; Wang, L.; Zhao, C.; Yang, W. *Polym. Chem.* **2016**, *7*, 4226−4236. (b) Yang, Q.; Dumur, F.; Morlet-Savary, F.; Poly, J.; Lalevée, J. *Macromolecules* **2015**, *48*, 1972−1980. (c) Konkolewicz, D.; Schröder, K.; Buback, J.; Bernhard, S.; Matyjaszewski, K. *ACS Macro Lett.* **2012**, *1*, 1219−1223. (d) Tasdelen, M. A.; Uygun, M.; Yagci, Y. *Macromol. Rapid Commun.* **2011**, *32*, 58−62.

(9) (a) Telitel, S.; Dumur, F.; Campolo, D.; Poly, J.; Gigmes, D.; Fouassier, J. P.; Lalevée, J. *J. Polym. Sci., Part A: Polym. Chem.* **2016**, *54*, 702−713. (b) Bansal, A.; Kumar, P.; Sharma, C. D.; Ray, S. S.; Jain, S. L. *J. Polym. Sci., Part A: Polym. Chem.* **2015**, *53*, 2739−2746. (c) Pan, X.; Malhotra, N.; Zhang, J.; Matyjaszewski, K. *Macromolecules* **2015**, *48*, 6948−6954.

(10) (a) Treat, N. J.; Fors, B. P.; Kramer, J. W.; Christianson, M.; Chiu, C.-Y.; Read de Alaniz, J.; Hawker, C. J. *ACS Macro Lett.* **2014**, *3*, 580−584. (b) Fors, B. P.; Hawker, C. J. *Angew. Chem., Int. Ed.* **2012**, *51*, 8850−8853.

(11) Isse, A. A.; Lin, C. Y.; Coote, M. L.; Gennaro, A. *J. Phys. Chem. B* **2011**, *115*, 678−684.

(12) Furst, L.; Matsuura, B. S.; Narayanam, J. M. R.; Tucker, J. W.; Stephenson, C. R. J. *Org. Lett.* **2010**, *12*, 3104−3107.

(13) Hu, J.; Wang, J.; Nguyen, T. H.; Zheng, N. *Beilstein J. Org. Chem.* **2013**, *9*, 1977−2001.

(14) Volz, D.; Wallesch, M.; Flechon, C.; Danz, M.; Verma, A.; Navarro, J. M.; Zink, D. M.; Brase, S.; Baumann, T. *Green Chem.* **2015**, *17*, 1988−2011.

(15) (a) Ding, M.; Jian, X.; Zhang, L.; Cheng, Z.; Zhu, X. *Macromol. Rapid Commun.* **2015**, *36*, 1702−1721. (b) Magenau, A. J. D.; Strandwitz, N. C.; Gennaro, A.; Matyjaszewski, K. *Science* **2011**, *332*, 81−84. (c) Matyjaszewski, K.; Jakubowski, W.; Min, K.; Tang, W.; Huang, J.; Braunecker, W. A.; Tsarevsky, N. V. *Proc. Natl. Acad. Sci. U. S. A.* **2006**, *103*, 15309−15314. (d) Faucher, S.; Okrutny, P.; Zhu, S. *Macromolecules* **2006**, *39*, 3−5.

(16) Romero, N. A.; Nicewicz, D. A. *Chem. Rev.* **2016**, *116*, 10075−10166.

(17) Miyake, G. M.; Theriot, J. C. *Macromolecules* **2014**, *47*, 8255−8261.

(18) (a) Treat, N. J.; Sprafke, H.; Kramer, J. W.; Clark, P. G.; Barton, B. E.; Read de Alaniz, J.; Fors, B. P.; Hawker, C. J. *J. Am. Chem. Soc.* **2014**, *136*, 16096. (b) Pan, X.; Lamson, M.; Yan, J.; Matyjaszewski, K. *ACS Macro Lett.* **2015**, *4*, 192−196. (c) Pan, X.; Fang, C.; Fantin, M.; Malhotra, N.; So, W. Y.; Peteanu, L. A.; Isse, A. A.; Gennaro, A.; Liu, P.; Matyjaszewski, K. *J. Am. Chem. Soc.* **2016**, *138*, 2411−2425.

(19) Theriot, J. C.; Lim, C.-H.; Yang, H.; Ryan, M. D.; Musgrave, C. B.; Miyake, G. M. *Science* **2016**, *352*, 1082−1086.

(20) Pearson, R. M.; Lim, C.-H.; McCarthy, B. G.; Musgrave, C. B.; Miyake, G. M. *J. Am. Chem. Soc.* **2016**, *138*, 11399−11407.

(21) (a) Lee, J.; Shizu, K.; Tanaka, H.; Nakanotani, H.; Yasuda, T.; Kaji, H.; Adachi, C. *J. Mater. Chem. C* **2015**, *3*, 2175−2181. (b) Uoyama, H.; Goushi, K.; Shizu, K.; Nomura, H.; Adachi, C. *Nature* **2012**, *492*, 234−238. (c) Tanaka, H.; Shizu, K.; Nakanotani, H.; Adachi, C. *Chem. Mater.* **2013**, *25*, 3766−3771.

(22) (a) Kalyanasundaram, K. *Coord. Chem. Rev.* **1982**, *46*, 159−244. (b) Flamigni, L.; Barbieri, A.; Sabatini, C.; Ventura, B.; Barigelletti, F. *Top. Curr. Chem.* **2007**, *281*, 143−203.

(23) Fukuzumi, S.; Kotani, H.; Ohkubo, K.; Ogo, S.; Tkachenko, N. V.; Lemmetyinen, H. *J. Am. Chem. Soc.* **2004**, *126*, 1600−1601.

(24) See Supporting Information for details.

(25) Morris, J. V.; Brühlmann, U.; Serafimov, O.; Huber, J. R. *Ber. Bunsenges. Phys. Chem.* **1974**, *78* (12), 1348−1353.

(26) Tao, Y.; Yuan, K.; Chen, T.; Xu, P.; Li, h.; Chen, R.; Zheng, C.; Zhange, L.; Huang, W. *Adv. Mater.* **2014**, *26*, 7931−7958.

(27) Lakowicz, J. R. *Principles of Fluorescence Spectrocopy*; Springer Science: New York, 2006.

(28) (a) Tanaka, H.; Shizu, K.; Nakanotani, H.; Adachi, C. *Chem. Mater.* **2013**, *25*, 3766−3771. (b) Grabowski, Z. R.; Rotkiewicz, K. *Chem. Rev.* **2003**, *103*, 3899−4032. (c) Borowicz, P.; Herbich, J.; Kapturkiewicz, A.; Opallo, M.; Nowacki, J. *Chem. Phys.* **1999**, *249*, 49−62.

(29) Marcus, Y.; Hefter, G. *Chem. Rev.* **2006**, *106*, 4585−4621.